Ultrasonic Imaging
2021, Vol. 43(5) 282–294

DOI: 10.1177/01617346211026350
journals.sagepub.com/home/uix
SAGE

Fourier-based Synthetic-aperture Imaging for Arbitrary Transmissions by Cross-correlation of Transmitted and Received Wave-fields

Rehman Ali[1]

Abstract

Investigations into Fourier beamforming for medical ultrasound imaging have largely been limited to plane-wave and single-element transmissions. The main aim of this work is to generalize Fourier beamforming to enable synthetic aperture imaging with arbitrary transmit sequences. When applied to focused transmit beams, the proposed approach yields a full-waveform-based alternative to virtual-source synthetic aperture, which has implications for both coherence imaging and sound speed estimation. When compared to virtual-source synthetic aperture and retrospective encoding for conventional ultrasound sequences (REFoCUS), the proposed imaging technique shows an 8.6 and 3.8 dB improvement in contrast over virtual source synthetic aperture and REFoCUS, respectively, and a 55% improvement in point target resolution over virtual source synthetic aperture. The proposed image reconstruction technique also demonstrates general imaging improvements in vivo, while avoiding limitations seen in prior techniques.

Keywords

Fourier beamforming, synthetic aperture, angular spectrum method, shot-profile migration, full waveform

Introduction

In medical ultrasound imaging, Fourier beamforming techniques often rely on diffraction, governed by the wave equation, to focus ultrasound channel signals into images. Previous work on Fourier beamforming has largely focused on high-frame rate imaging with plane-wave transmissions.[1-7] These approaches often use k-space and frequency-domain representations for plane wave transmissions into the medium to develop approximations that lead to fast and closed-form imaging techniques.

Notably, the f–k Stolt's migration approach[6] to plane-wave imaging is based on the exploding reflector model,[8] which uses a single geophone as both a source and receiver. Rather than develop an exact formulation for plane-wave imaging, the approach in Garcia et al.[6] re-parameterizes Stolt's migration so that the effective receive delays induced by Stolt's migration best matches the exact receive delays needed for standard delay-and-sum beamforming with plane waves. The unmodified exploding reflector model would correspond exactly to monostatic synthetic aperture imaging, in which each individual element is used to transmit and receive signal. As a result, f–k Stolt's migration with the exploding reflector model yields fast and accurate image reconstruction for monostatic synthetic aperture channel data. Recent work in Moghimirad et al.[9] extends Fourier beamforming to the multistatic synthetic aperture, in which receive channel data from every receive element is captured for each single-element transmission.

Although ultrasound channel signals are typically captured from focused transmit beams rather than single-element transmits due to their low SNR, retrospective encoding for conventional ultrasound sequences (REFoCUS)[10-14] provides a framework for recovering multistatic synthetic aperture channel data from transmit beams with arbitrary transmit delays and apodization. Since REFoCUS enables recovery of the multistatic dataset, the Fourier beamforming approach in Moghimirad et al.[9] is enabled by REFoCUS.

Virtual source synthetic aperture[15] treats the focus of a focused transmit beam as a virtual element or source. However, this virtual source approach is not applicable to imaging locations outside of the lateral extent of the beam. As a result, the number of focused-transmit beams contributing to an image

[1]Stanford University, Palo Alto, CA, USA

Corresponding Author:
Rehman Ali, Stanford University, 3155 Porter Dr, Palo Alto, CA 94304, USA.
Email: rali8@stanford.edu

point decreases as the image point approaches the transmit focus, resulting in imaging artifacts around the focus. Furthermore, it can be difficult to account for the effects of phase aberration and sound speed error when virtual source synthetic aperture is applied to focused transmit beams because virtual source synthetic aperture assumes perfect focusing at pre-defined focal locations that act as virtual sources. Although Fourier beamforming has been extended to virtual source synthetic aperture,[16] it inherits all of the major drawbacks of virtual sources because of its shared assumptions.

Ultimately, the main goal of REFoCUS is to be able to convert channel data from as wide a variety of transmit sequences as possible to a common multistatic dataset that enables optimal focusing at all locations in space and circumvents the need for virtual sources. As a result, REFoCUS enables synthetic aperture imaging without the drawbacks associated with virtual sources. If REFoCUS could recover the multistatic dataset from any arbitrary set of transmissions, REFoCUS would unite all of ultrasound imaging under a single unified framework. However, the recoverability of the multistatic dataset is largely limited by the sampling and coverage of transmit beams in k-space.[13] In many cases, the number of transmit beams per frame is limited by the desired frame rate, which can further limit the recoverability of the multistatic dataset.

The main goal of this work is to demonstrate a unifying framework that provides a single imaging technique that optimally focuses ultrasound channel data from any arbitrary transmit sequence. This approach avoids the drawbacks associated with virtual source synthetic aperture and circumvents the need to recover a multistatic dataset. The proposed framework is based on a Fourier-domain implementation of a seismic imaging technique known as shot-profile migration.[17-23]

Theory

Angular Spectrum Method

Ultrasonic wave-fields $p(x,z,f)$ as a function of location (x,z) and frequency f can be propagated from a depth of z to $z+\Delta z$ using the angular spectrum method:

$$p(x,z+\Delta z,f) = W(x)\mathcal{F}^{-1}_{k_x \mapsto x}\{H_{\pm}(k_x,\Delta z,f)\;\mathcal{F}_{x\mapsto k_x}[p(x,z,f)](k_x,z,f)\}(x,z+\Delta z,f), \tag{1}$$

where $H_{\pm}(k_x,\Delta z,f)$ is the propagator[24] given by

$$H_{\pm}(k_x,\Delta z,f) = \exp\left(\pm j2\pi\left(\frac{f^2}{c^2}-k_x^2\right)^{1/2}\Delta z\right). \tag{2}$$

The window function $W(x)$ is used to suppress the wrap-around artifacts caused by the discrete implementation of Fourier transform, and c is the speed of sound in the medium. The forward and inverse Fourier transform operators $\mathcal{F}_{x\mapsto k_x}$ and $\mathcal{F}^{-1}_{k_x\mapsto x}$ in the lateral dimension are

$$\mathcal{F}_{x\mapsto k_x}[f(x)](k_x) = \int_{-\infty}^{\infty} f(x)e^{-j2\pi k_x x}dx, \tag{3}$$

$$\mathcal{F}^{-1}_{k_x\mapsto x}\{\hat{f}(k_x)\}(x) = \int_{-\infty}^{\infty} \hat{f}(k_x)e^{j2\pi k_x x}dk_x. \tag{4}$$

Imaging by Correlating Transmit and Receive Wave-fields

In seismic imaging, the imaging condition[18-20] states that an image $I(x,z)$ can be formed by summing the time- or frequency-domain cross-correlation of transmit $p_{tx(i)}(x,z,t)$ and receive $p_{rx(i)}(x,z,t)$ wave-fields for N transmit events:

$$I(x,z) = \sum_{i=1}^{N} I_i(x,z) \tag{5}$$

where

$$\begin{aligned} I_i(x,z) &= \int_{-\infty}^{\infty} p^*_{tx(i)}(x,z,t)\,p_{rx(i)}(x,z,t)dt \\ &= \int_{-\infty}^{\infty} p^*_{tx(i)}(x,z,f)\,p_{rx(i)}(x,z,f)df. \end{aligned} \tag{6}$$

The transmit $p_{tx(i)}(x,z,f)$ and receive $p_{rx(i)}(x,z,f)$ wave-fields are calculated recursively according to

$$p_{tx(i)}(x,z+\Delta z,f) = W(x)\mathcal{F}^{-1}_{k_x\mapsto x}\{H_-(k_x,\Delta z,f)\;\mathcal{F}_{x\mapsto k_x}[p_{tx(i)}(x,z,f)](k_x,z,f)\}, \tag{7}$$

$$p_{rx(i)}(x,z+\Delta z,f) = W(x)\mathcal{F}^{-1}_{k_x\mapsto x}\{H_+(k_x,\Delta z,f)\;\mathcal{F}_{x\mapsto k_x}[p_{rx(i)}(x,z,f)](k_x,z,f)\}, \tag{8}$$

where $p_{tx(i)}(x,z=0,f)$ and $p_{rx(i)}(x,z=0,f)$ represents the frequency spectra of the transmit pulse and receive channel data from each element on the array (located at $z=0$). Knowledge of the transmit pulse spectrum $P(f)$, transmit focal delays $\tau_i(x)$, and transmit apodization $A_i(x)$ for each transmit event i is used to form $p_{tx(i)}(x,z=0,f)$:

$$p_{tx(i)}(x,z=0,f) = A_i(x)P(f)e^{-j2\pi f\tau_i(x)}. \tag{9}$$

The image formation approach described in this section will be referred to as shot-profile migration in the remainder of this work.

Methods

Simulations in Field II

Radio-frequency channel data for the walking aperture focused-transmit sequence described in Table 1 was simulated in Field II[25,26] for a medium of random diffuse point scatterers whose reflectivities were modified to simulate anechoic lesions and point targets in a uniform speckle background. Radio-frequency channel data for the plane-wave

Table 1. Walking-Aperture Focused-Transmit Sequence in Field II Simulation.

Parameter	Value	Units
Array geometry	Linear	—
Number of elements	128	Elements
Element pitch	0.2	mm
Center frequency	6	MHz
Fractional bandwidth (−6 dB)	70%	—
Focal depth	20	mm
Transmit angle	0	Degrees
Beam origin range	[−12.8, 12.8]	mm
Beam origin step	1	Element
Aperture width	64	Elements
Transmit apodization	Rectangular	—

Table 2. Plane-Wave Transmit Sequence in Field II Simulation.

Parameter	Value	Units
Array geometry	Phased	—
Number of elements	96	Elements
Element pitch	0.154	mm
Center frequency	5	MHz
Fractional bandwidth (−6 dB)	70%	—
Transmit angles	−10, −9.5, . . ., 9.5, 10	Degrees
Aperture width	96	Elements
Transmit apodization	Rectangular	—

transmit sequence described in Table 2 was also simulated in Field II for a diffuse scattering medium with an anechoic lesion.

Experimental Data Acquisition

Table 3 summarizes the walking-aperture focused-transmit sequence implemented on a Siemens research scanner with an L10-4 probe. Radiofrequency channel data were acquired in vivo from the thyroid and carotid of a healthy human volunteer under an IRB-approved protocol, and written informed consent was obtained.

Radio-frequency channel data from a plane-wave sequence, consisting of seven tilted plane waves whose angular span ranged from −1.5° to 1.5° (0.5° steps), for an in vitro phantom with point targets was obtained from the supplemental materials in Garcia et al.[6] See Garcia et al.[6] for complete details regarding the probe, acquisition system, and phantom information.

Imaging Techniques

Shot-Profile Migration is first demonstrated in the time domain, but is implemented in the frequency domain for the remainder of this work. Shot-Profile Migration is compared to dynamic-receive focusing, virtual source synthetic

Table 3. Walking-Aperture Focused-Transmit Sequence on Siemens 10L4.

Parameter	Value	Units
Array geometry	Linear	—
Number of elements	192	Elements
Element pitch	0.201	mm
Focal depth	20	mm
Transmit angle	0	Degrees
Beam origin range	[−19.3, 19.3]	mm
Beam origin step	0.19442	mm
Aperture width	9.779	mm
Transmit apodization	Half-circle	—

aperture,[15] and the adjoint-based REFoCUS[10,11,13] scheme for the walking-aperture focused-transmit sequences. Edge waves produced at the edges of the transmit aperture are also incorporated into the virtual source synthetic aperture image reconstruction as was done in Bottenus[27] to enable reconstruction outside the lateral extent of the focused-transmit beam. Shot-Profile Migration is also compared to f–k Stolt's migration[6] and REFoCUS for the plane wave transmit sequences.

In some cases, reconstructed B-mode images are displayed at 80 dB, which is larger than the dynamic range typically used in in clinical imaging, in order to better highlight difference between the reconstruction techniques. Point target resolution, and lesion contrast are used to assess each imaging technique.

Results

Figure 1 illustrates shot-profile migration, which is the time-domain cross-correlation of transmitted and back-propagated receive wave-fields. The transmitted wave-field propagates into the medium as the receive wave-field, which was back-propagated into the medium, travels upward toward the transducer. As the upward-going receive wave-field spatially intersects the downward-going transmit wave-field as a function of time, the time-domain cross correlation forms the ultrasound image prior to amplitude detection and decibel-scaling. This procedure does not apply any focal delays to receive signals when forming the receive wave-field because this is accomplished by back-propagating receive signals into the medium. According to equation (6), the time-domain cross-correlation can also be implemented in the frequency domain. All remaining results demonstrate the frequency-domain implementation of shot-profile migration

Figure 2 compares shot-profile migration to virtual source synthetic aperture. Figure 2(a) shows virtual source synthetic aperture reconstructions for each individual transmit beam as well as after coherent compounding. Figure 2(b) uses the edge waves to laterally extend the virtual source reconstructions of each transmit beam. Figure 2(c) shows that shot-profile migration naturally achieves the laterally extended

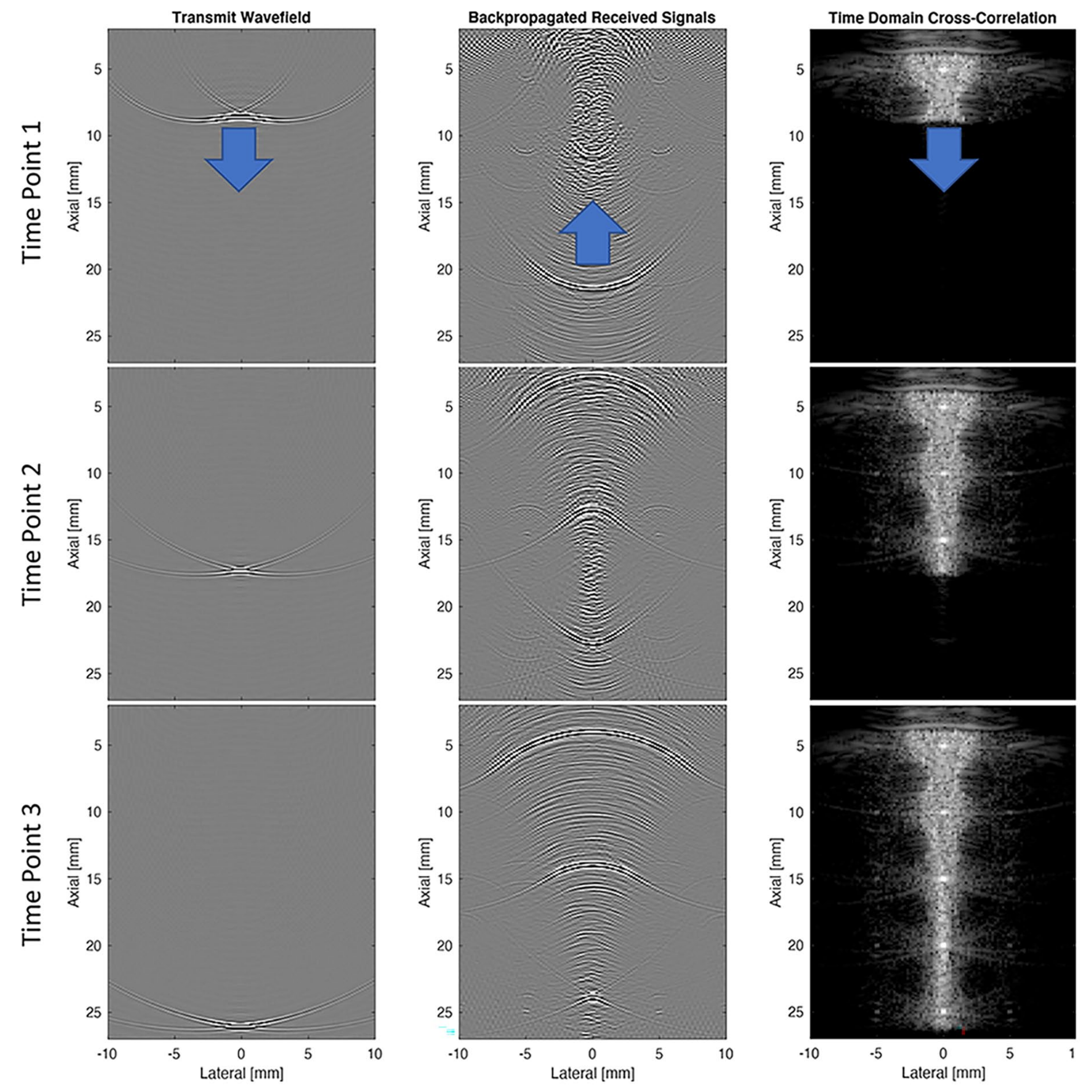

Figure 1. Shot-profile migration by time domain cross-correlation of transmit beam wave-field with the backpropagated wave-field for received signals. The wave-field for the transmit beam propagates into the medium as the wave-field for receive signals propagates toward the transducer line. Only the real components of the wave-fields are shown here. The time-domain cross correlation of complex-valued transmit and receive wave-fields creates the ultrasound image prior to amplitude detection and display on a decibel scale (80 dB dynamic range shown here).

view from each individual transmit beam based on the cross-correlation of transmitted and received wave-fields.

Figure 3 shows dynamic receive focusing, virtual source synthetic aperture with and without edge waves, REFoCUS, and shot-profile migration in the thyroid and carotid. The virtual source reconstruction (Figure 3(b)) appears to improve focusing throughout the image over conventional dynamic receive focusing (Figure 3(a)). In this in vivo example, edge waves (Figure 3(c)) appear to only add noise to the virtual source reconstruction. Both REFoCUS (Figure 3(d)) Shot-profile migration (Figure 3(e)) appear to improve focusing over conventional dynamic-receive focusing while retaining a more uniform illumination at all depths in the ultrasound image as compared to the virtual source reconstruction without edge waves (Figure 3(b)). However, while REFoCUS (Figure 3(d)) appears to add clutter to the reconstructed in image in the near field, shot-profile migration (Figure 3(e)) does not appear to suffer from this.

Figure 4 shows virtual source synthetic aperture (with edge-waves), REFoCUS, and shot-profile migration as a function of the beam sampling. Downsampling beams by a factor of four results in a banding artifact at the focus in the virtual source reconstruction but only minor and negligible changes in REFoCUS and shot-profile migration. Downsampling by

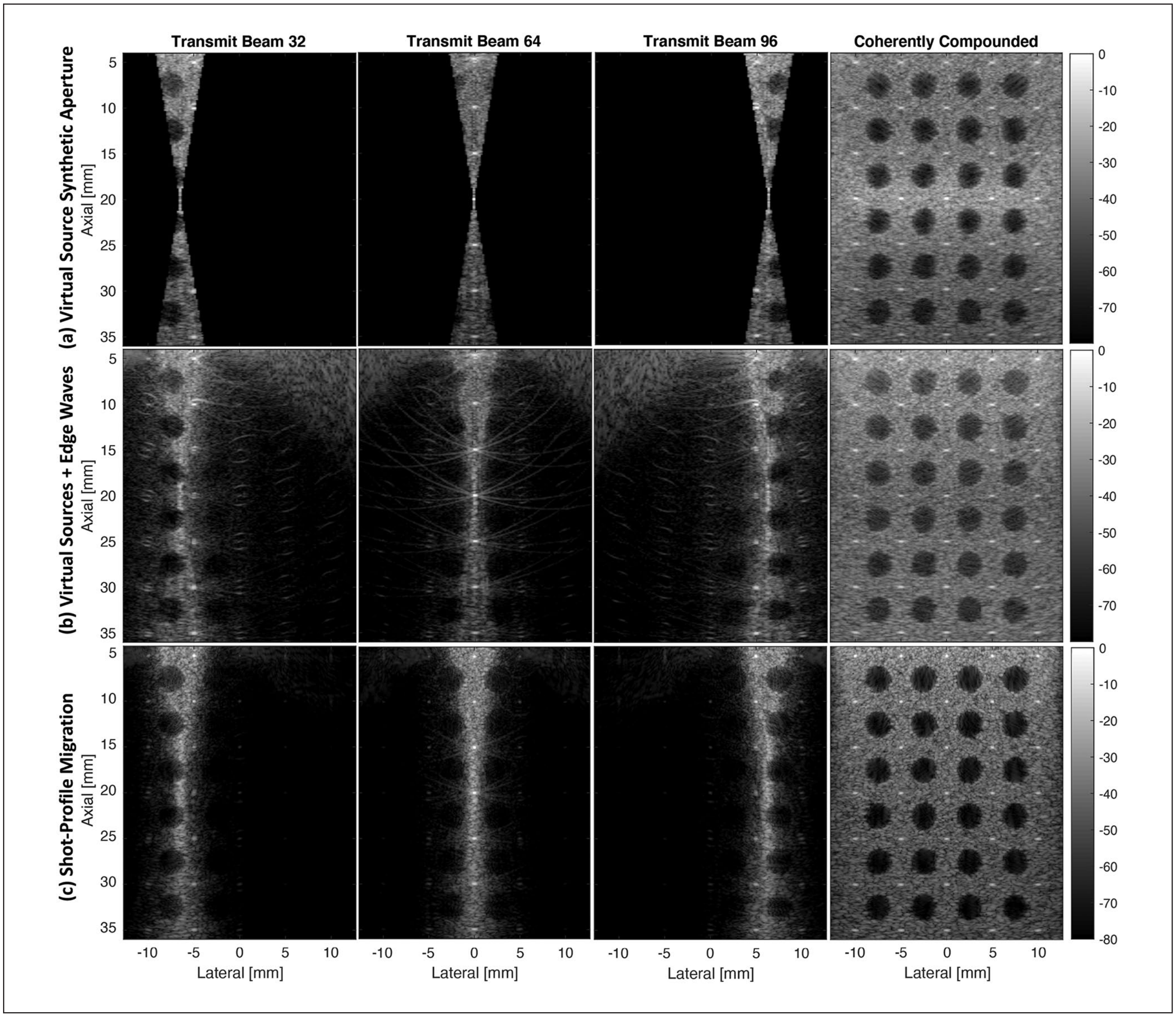

Figure 2. Synthetic aperture imaging based on (a) virtual sources, (b) virtual sources with edge waves, and (c) shot-profile migration. In comparison to (a), the edge waves in (b) laterally extend the field of view from each transmit beam. Shot-profile migration in (c) naturally provides the same lateral extension via the cross-correlation process shown in Figure 1, which is implemented here in the frequency domain rather than in the time domain.

a factor of eight results in a banding artifact in all three image reconstructions. Figure 5 highlights the reconstructions of the point targets at 15 mm depth using all the beams in the sequence. The shot-profile migration and REFoCUS reconstructions have nearly identical resolution and both improve resolution over the virtual source reconstruction by 55%. Figure 6 highlights the reconstructions of the lesions at 17.5 mm depth using all the beams in the transmit sequence. The red and blue circle indicate the regions over which contrast was computed. Shot-profile migration achieves the highest contrast, followed by REFoCUS and the virtual source reconstruction. The contrast achieved by shot-profile migration exceeds that of REFoCUS and the virtual source reconstruction by 3.8 and 8.6 dB, respectively. Figure 7 shows virtual source synthetic aperture, REFoCUS, and shot-profile migration as a function of the beam sampling in vivo. Edge waves were not included in these virtual source reconstructions because edge waves only appear to add noise to the reconstructed images in the in vivo example (Figure 3(c)). Thus, shot-profile migration is shown alongside the virtual source reconstruction without edge waves to provide a more fair comparison.

Shot-profile migration is also compared to f–k Stolt's migration and REFoCUS for imaging with plane-waves.

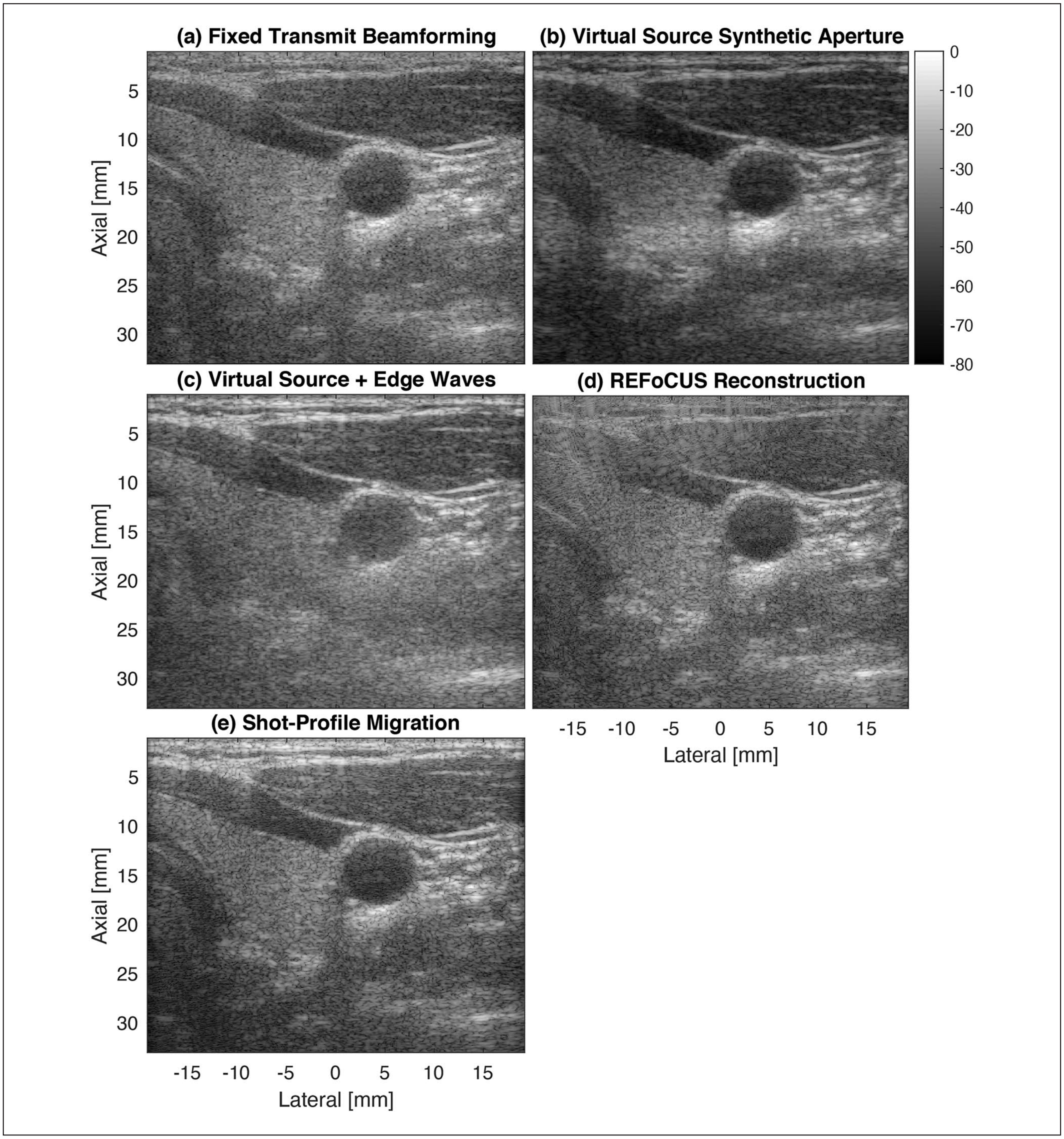

Figure 3. Image formation in vivo. (a) Fixed-focus transmit dynamic-receive beamforming. (b) Virtual source synthetic aperture. (c) Virtual source synthetic aperture with edge waves, (d) REFoCUS. (e) Shot-profile migration. All images are shown here at 80 dB dynamic range.

Note that although f–k migration is only applicable to plane-wave and monostatic synthetic aperture image reconstructions, shot-profile migration can be used to reconstruct images with any arbitrary transmit sequence. Here, we demonstrate plane-wave imaging examples to further demonstrate the generality of shot-profile migration and compare shot-gather migration to f–k migration, which was previously introduced to medical ultrasound for its application to plane-wave imaging. Figure 8 shows shot-profile migration, f–k Stolt's migration, and REFoCUS images of an

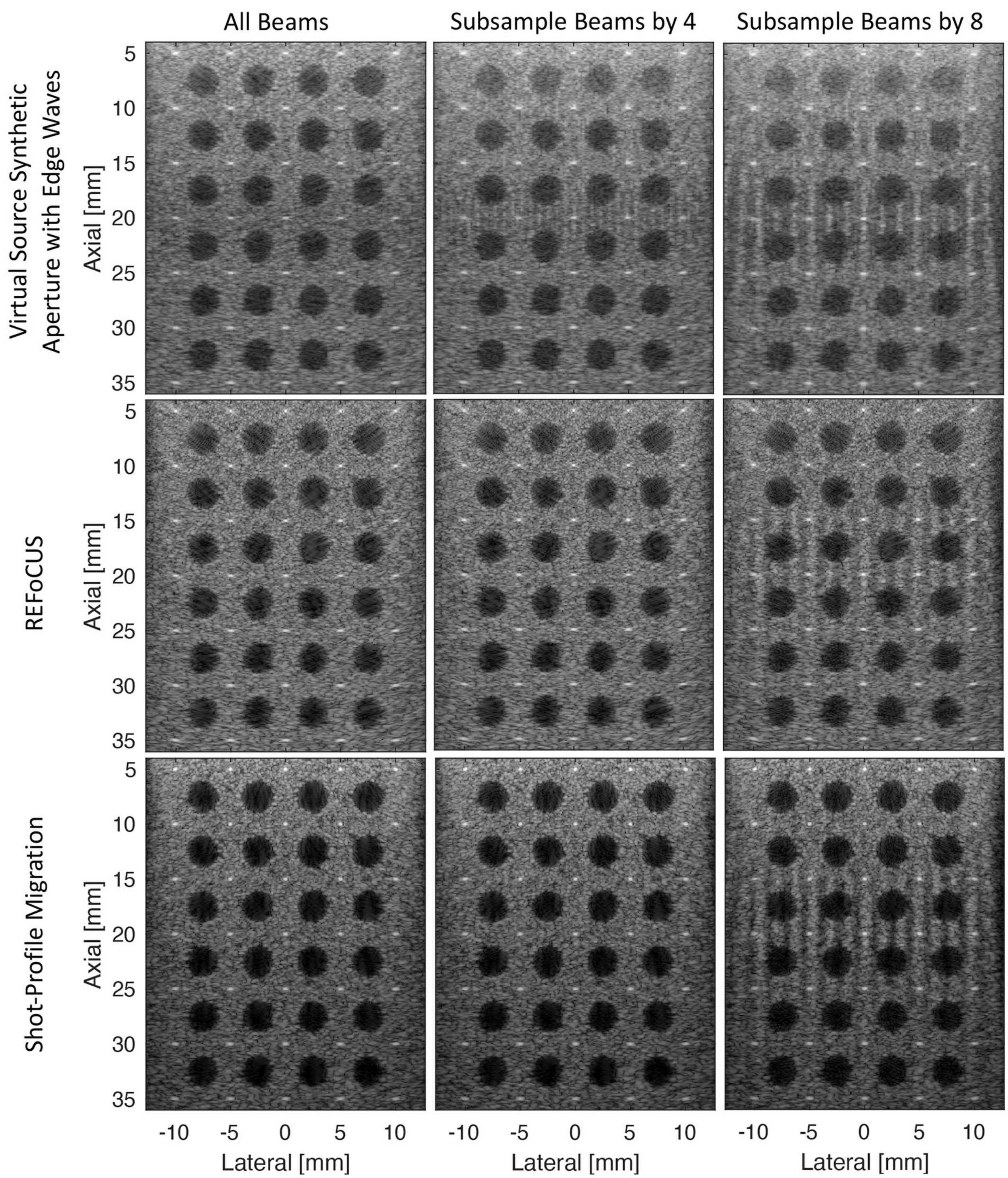

Figure 4. Effect of beam spacing on virtual source synthetic aperture (with edge waves), REFoCUS, and shot-profile migration. All images are shown here at 80 dB dynamic range.

in vitro point target phantom insonified by seven plane waves, whose angles range from −1.5 to 1.5 degrees. The results of shot-profile and f–k Stolt's migration show significant agreement with one another, and there is no significant difference in the point target resolution between the two migration techniques; however, REFoCUS appears to struggle with image reconstruction in the near field. Figure 9 shows how lesion contrast for each of the three imaging

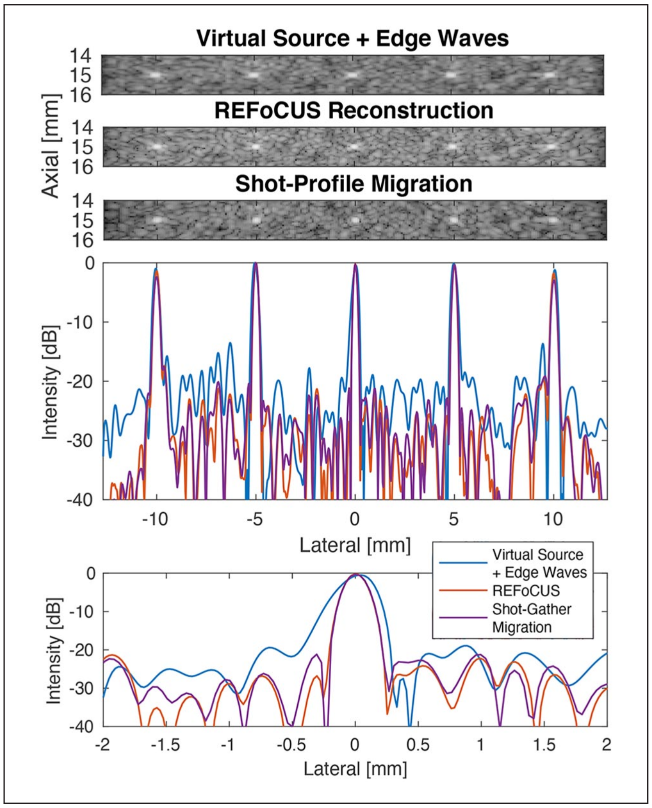

Figure 5. Comparison of point target imaging in virtual source synthetic aperture (with edge waves), REFoCUS, and shot-profile migration. The full-width at half-maximum for the center-most point target at 15 mm depth is 0.396 mm for virtual source synthetic aperture, 0.256 mm for multistatic synthetic aperture with REFoCUS, and 0.256 mm for shot-profile migration. All images are shown here at 80 dB dynamic range.

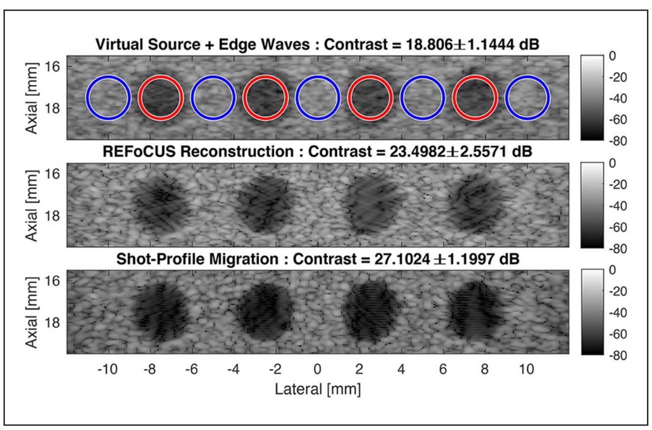

Figure 6. Comparison of Lesion contrast in virtual source synthetic aperture (with edge waves), REFoCUS, and shot-profile migration. For each of the four lesions, contrast is measured between the region circled in red (the anechoic lesion) and two of the neighboring regions circled in blue (the background speckle). The mean and standard deviation across the four contrast measurements is reported for each image reconstruction technique.

techniques changes as a function of the angular span of plane waves coherently summed to form the ultrasound image. As the angular span of the plane wave sequences increases, the lesion contrast of each imaging technique also increases. Shot-profile migration appears to have the highest contrast, followed by REFoCUS and f–k Stolt's migration.

Discussion

The time-domain cross-correlation imaging technique illustrated in Figure 1 typically goes by reverse-time, shot-profile, or shot-gather migration in seismic imaging.[18-22] This technique is typically implemented in reverse-time where the the transmit event is played backward in time while the received wave-field is propagated back into the medium. As a result the cross correlation is typically performed in reverse time, and the image forms upward toward the surface where the sources and receivers are located, rather than downward and away from transducer surface as in Figure 1. Regardless of the direction of the time, the cross-correlation process achieves an image reconstruction that is automatically receive-focused at all imaging points because the back-propagated receive signals will converge back to the locations where they were back-scattered as the transmit wave-field passes over them.

This technique is also known as shot-gather migration because the received signal for each shot, or transmit event, are gathered and back-propagated into the medium alongside the transmit event. The partial images from each shot are summed, yielding the final image reconstruction as shown in Figure 2(c). However, the image reconstructions in Figure 2(c), are performed in the frequency domain rather than the time domain based on the frequency-domain implementation of the cross correlation process (see equation (6) in the Theory section). This imaging technique is implemented in the frequency domain because all wave-fields are propagated using the angular spectrum method. The angular spectrum method is typically referred to as downward continuation[28,29] in seismic imaging because it is typically thought of as a continuation of source and receiver wave-fields downwards into the medium.

Image reconstruction techniques like shot-profile migration are not common in medical ultrasound imaging because delay-and-sum approaches can be implemented much more quickly. For example, the virtual source reconstructions in Figures 2(a) and (b), with and without edge-waves, is implemented by delaying receive signals according to the expected times of flight in the medium. In the case of Figure 2(b), this is done by assembling receive delays for the central support of the beam and the two edge waves lateral to the main support of the beam. This results in three different images: one image for the main support of the beam (Figure 2(a)), and images for each of the two edge waves, which are compounded into main-support image. The final result of compounding the main support of the beam with the edge waves

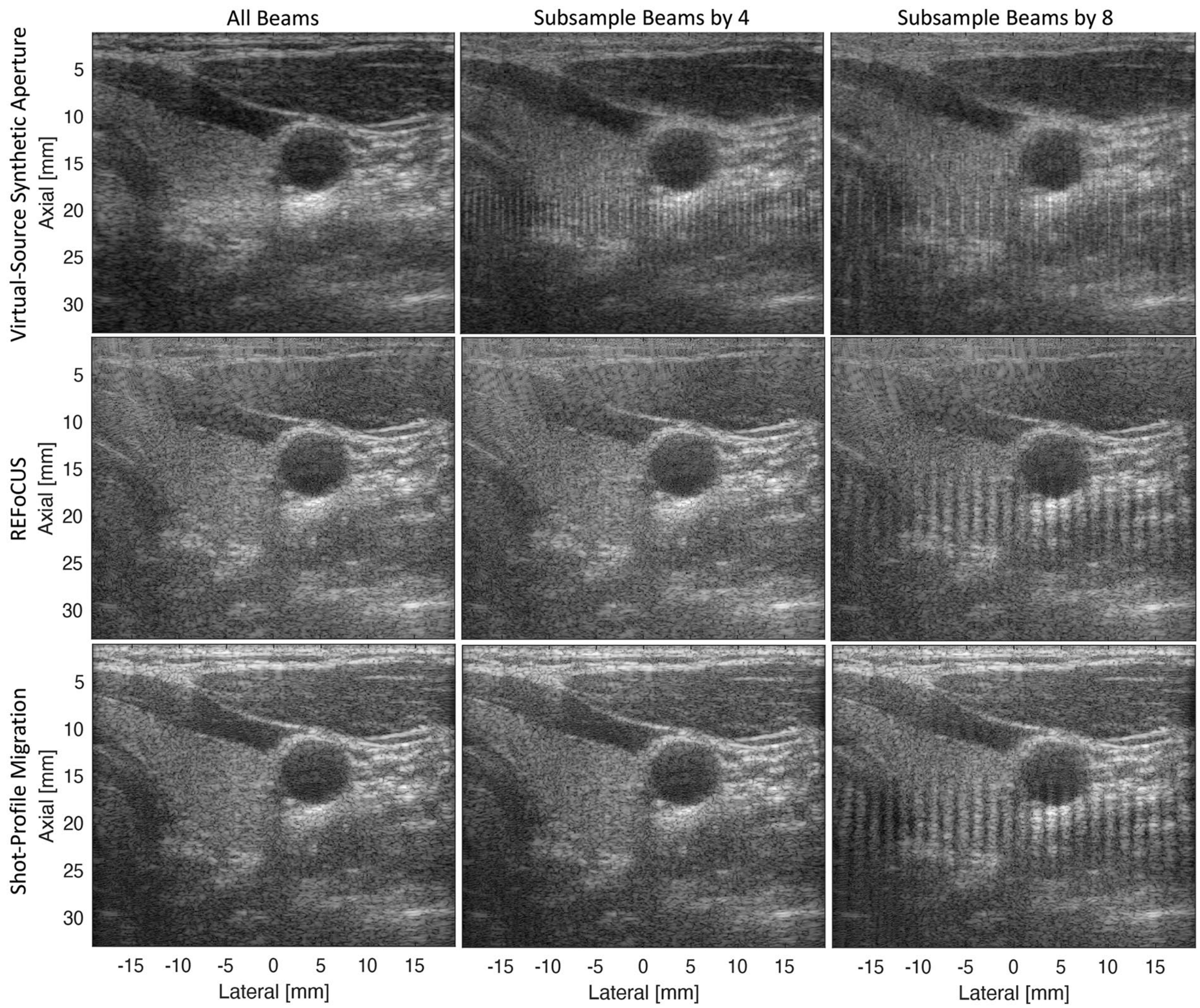

Figure 7. In vivo comparison of virtual source synthetic aperture, REFoCUS, and shot-profile migration in the presence of increasing beam sparsity. All images are shown here at 80 dB dynamic range.

is shown in Figure 2(b). This process is highly discrete as it resolves images for each of three distinct components of the transmitted wave.

However, as seen in Figure 1, the three components of the wave are not distinct; rather, they overlap with each other, and there is a smooth transition between these components of the transmitted wavefront. The continuous nature of the transmitted wave-field is better modeled by the shot-profile migration method introduced in this work. As a result, although both virtual source reconstruction (after adding the contribution of edge waves to the image) and shot-profile migration can form images outside the main support of the beam, the virtual source reconstruction degrades more quickly when the beams are subsampled as in Figure 4. Furthermore, edge-waves only appear to add noise to the virtual source reconstruction in Figures 3(b) and (c) due to the half-circle transmit apodization. This transmit apodization decreases the intensity of the edge waves and further smoothens the transition between the main support of the beam and the edge waves. In this case, the addition of edge waves only adds clutter to the virtual source reconstruction, while shot-profile migration (Figure 3(e)) accurately accounts for apodization in the transmit waveform during image reconstruction. Note that this is not the case in Figure 2 where rectangular apodization is used and edge waves are more distinct.

Another imaging technique that improves upon virtual source synthetic aperture in terms of both resolution and contrast (Figures 5 and 6, respectively) is REFoCUS. This imaging technique isolates the single-element contributions to a multistatic synthetic aperture dataset from channel data collected from a focused-transmit sequence and performs a

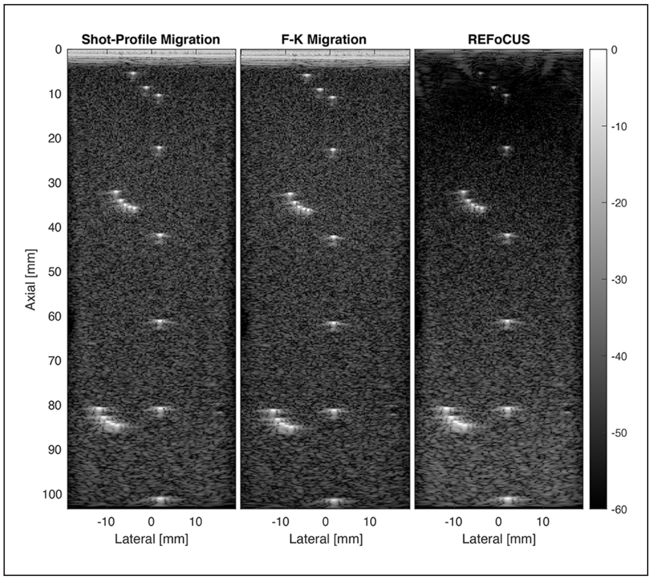

Figure 8. Comparison of shot-profile migration, f–k Stolt's migration, and REFoCUS on plane-wave channel data from in-vitro point target phantom provided by Garcia et al.[6] Results of shot-profile migration and f–k Stolt's migration are comparable with no significant difference in point target resolution. However, REFoCUS reconstruction is unable to reconstruct in the near field without significant reconstruction artifacts.

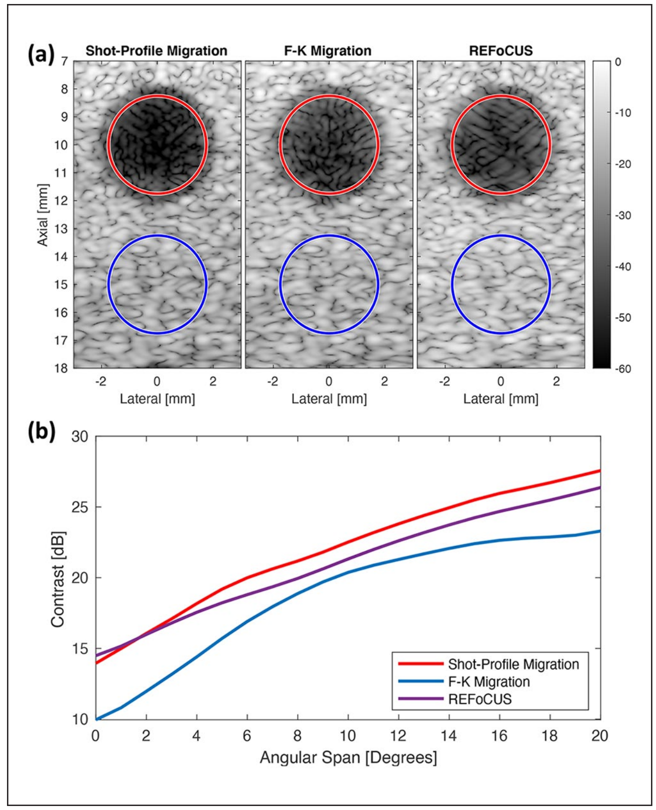

Figure 9. Lesion contrast in shot-profile migration, f–k Stolt's migration, and REFoCUS as a function of the angular span of the plane-wave transmit sequence. (a) Image reconstructions from each technique using the full angular span (20°) of the plane wave transmit sequence. The regions of interest used in computing the contrast are circled in red and blue. (b) Lesion contrast versus the angular span of transmits used for each of the three image reconstruction techniques.

multistatic synthetic aperture reconstruction. The intermediate step in REFoCUS is recovery of the multistatic dataset. Recent works[12,13] aim to improve upon the original implementation of REFoCUS[10,11] by applying a regularized inversion strategy as opposed to an adjoint strategy during the recovery process. Although the regularized inversion strategy improves the accuracy of the recovered multistatic dataset and generally improves resolution, the regularized inversion approach is also less robust to noise and beam sparsity. For this reason, REFoCUS is implemented in this work based on the adjoint approach originally introduced in Bottenus.[10,11]

Although both REFoCUS and the shot-profile migration approach improve upon the virtual source reconstruction in terms of both resolution and contrast (Figures 5 and 6), shot-profile migration further improves contrast beyond the REFoCuS reconstruction (Figure 6). When REFoCUS and shot-profile migration are applied in vivo (Figure 7), the main difference appears to be clutter throughout the REFoCUS image, especially in the near field. The presence of clutter in the REFoCUS reconstruction may be attributed to transmit apodization in the walking aperture transmit sequence. As previously shown in Ali et al.,[12,13] the adjoint-based REFoCUS may result in near-field artifacts and clutter due to inaccuracies in the recovered multistatic dataset when applied to a walking aperture transmit sequence; similar issues are also seen in the plane-wave imaging example shown in Figure 8. Regularized inversion was proposed in Ali et al.[12,13] in order to better account for a changing transmit apodization between transmit events when recovering the multistatic dataset. However, the half-circle transmit apodization in this in vivo example makes accurate recovery of the multistatic dataset more difficult. It is also interesting to note that when REFoCUS is compared to virtual source synthetic aperture and shot-profile migration (Figures 4 and 7), REFoCUS results in the same banding artifact at the focus as seen in both the virtual source synthetic aperture and shot-profile migration when the beams are downsampled by a factor of 8. This is because although the goal of REFoCUS is to recover the multistatic dataset, REFoCUS is ultimately limited by the k-space coverage of the original transmit sequence used to acquire the channel data.[13] Since all three imaging techniques rely on the same underlying transmit sequence for image reconstruction, they each degrade in a similar way when the transmit beams are undersampled. Previous work has also demonstrated the similarity of REFoCUS and virtual source reconstructions when imaging with phased arrays.[30]

Shot-profile migration circumvents the need to recover the multistatic dataset by working directly with the transmit sequence used to acquire the channel data. Additionally, shot-profile migration also creates new opportunities for sound speed estimation. Previously, sound speed estimation techniques have largely been limited to multistatic synthetic aperture[31,32]) and plane wave acquisitions[33,34] because these specific acquisitions simplify ray-based approaches to sound speed reconstruction. However, shot-profile migration is directly parameterized by sound speed and can be applied to any arbitrary transmit sequence. The form of the angular spectrum method presented in this work can account for axial variations in sound speed. Lateral variations in sound speed can also be incorporated into the angular spectrum method via a phase screen at the end of each depth-step.[7,35,36] Because the image reconstruction from this technique is parameterized by sound speed, the image reconstruction may be optimized with respect to sound speed to perform sound speed estimation and achieve distributed aberration correction. Attenuation may be incorporated into the angular spectrum method to provide a depth-gain compensation. This could be implemented as part of a phase screen after each depth step of the angular spectrum method. However, this also has the potential to amplify noise in the far field. Attenuation also generally results in a downward shift in the center frequency as a function of depth. This downward shift in center frequency and low signal-to-noise ratio can make accurate sound speed estimation more challenging deeper in the medium. In seismic imaging, there is a similar image-based optimization framework for sound speed estimation known as wave-equation migration velocity analysis (WEMVA).[37] Translation of WEMVA to medical ultrasound imaging is ultimately challenged by the diffuse nature of backscatter in the human body. The objective functions and overall methodology of WEMVA may need significant modifications for robust performance in medical ultrasound imaging.

Although the shot-profile migration technique introduced in this work ultimately overcomes many limitations of the preexisting synthetic aperture reconstruction techniques, its major limitation is its computational expense. For example, on an Intel Core i5 system (2.7 GHz) with 8GB of RAM, a reconstruction that requires 30 and 50 seconds using virtual source synthetic aperture (without edge-waves) and REFoCUS, respectively, requires approximately 130 seconds using shot-profile migration. The main source of computational expense in our implementation of shot-profile migration is the angular spectrum method. For an image reconstruction that is N_x points laterally and N_z points axially, the angular spectrum method for shot-profile migration requires $\mathcal{O}(N_f N_z N_x N \log N_x)$ operations, where N_f is the number of frequency bins in f. Each depth step in z of the angular spectrum method requires $N_f N_x N$ storage for the transmit and receive wave-fields. A virtual source reconstruction requires $\mathcal{O}(N_{rx} N_z N_x N)$ operations, where N_{rx} is the number of receive signals for each transmit event. When applying receive delays to channel signals, the interpolation of signals from distant locations in memory also results in memory latency as well. Despite this additional memory latency, virtual source synthetic aperture requires far fewer computations per imaging point. Certain computational schemes and processing architectures that can quickly perform a large number of FFTs in parallel and handle the storage requirements for the downward propagation of transmit and receive signals may yield the necessary speed-up for real-time imaging with the shot-profile migration. For example, shot-profile migration may be parallelized across transmit events and frequencies. However, the depth-stepping needed for the angular spectrum method must be a serial process. Software beamforming on clinical scanners presents the opportunity to implement more advanced image reconstruction techniques beyond conventional delay-and-sum beamforming. Shot-profile migration on clinical scanners may also provide new avenues for sound speed estimation and phase aberration correction in medical ultrasound imaging.

The goal of this work was to present shot-profile migration as a unifying framework that provides a single imaging technique that optimally focuses ultrasound channel data from any arbitrary transmit sequence. This work specifically demonstrated the application of shot-profile migration to channel data from focused transmit beams and plane waves. In these imaging cases, shot-profile migration improved upon the pre-existing imaging techniques in terms of point target resolution (Figure 5) and contrast (Figures 6 and 9). Shot-profile migration was shown to avoid the drawbacks of virtual source synthetic aperture aperture, such as the illumination changes seen at the focus (Figures 2(a) and 3(b)), while remaining more robust to beam sparsity (Figures 4 and 7). Shot-profile migration was also shown to avoid the near-field imaging artifacts seen in REFoCUS (Figures 3(d), 7, and 8) when applied to large linear arrays. Unlike REFoCUS, shot-profile migration does not require the recovery of a multistatic dataset to perform image reconstruction. Additionally, because shot-profile migration is parameterized by the sound speed in the medium via the angular spectrum method, shot-profile migration may open new avenues for sound speed estimation and distributed aberration correction techniques for pulse-echo ultrasound imaging.

Conclusions

This work introduces a Fourier-based synthetic aperture image reconstruction technique that overcomes many of the limitation of traditional synthetic aperture techniques. The proposed imaging technique, also known as shot-profile migration in seismic imaging, can be applied to acquisitions from any transmission sequence and opens new possibilities in the areas of sound speed reconstruction and phase aberration correction. Shot-profile migration is shown to improve imaging resolution and contrast over retrospective encoding for conventional ultrasound sequences (REFoCUS) and virtual source synthetic aperture image reconstruction. This work also demonstrates the robustness of shot-profile migration to beam sparsity both in simulation and in vivo. In order to make our efforts more accessible to the broader research community, we have provided sample channel data and code at github.com/rehmanali1994/FourierDomainBeamformer (DOI: 10.5281/zenodo.4606905).

Acknowledgments

The author would like to thank Joseph Jennings, Rustam Akhmadiev, and Dr. Biondo Biondi from the Department of Geophysics at Stanford University and Dr. Jeremy Dahl from the Department of Radiology at Stanford University for their valuable scientific discourse. The author would also like to thank Rick Loftman, Ismayil Guracar, and Vasant Salgaonkar at Siemens Healthineers for enabling in vivo demonstration of this work using channel data captured on a clinical scanner.

Declaration of Conflicting Interests

The author(s) declared no potential conflicts of interest with respect to the research, authorship, and/or publication of this article.

Funding

The author(s) disclosed receipt of the following financial support for the research, authorship, and/or publication of this article: Funding was provided by the National Defense Science and Engineering Graduate (NDSEG) fellowship.

ORCID iD

Rehman Ali https://orcid.org/0000-0003-2168-7895

References

1. Lu J-y. 2D and 3D high frame rate imaging with limited diffraction beams. IEEE Trans Ultrason Ferroelectr Freq Control. 1997;44(4):839-56.
2. Lu J-y. Experimental study of high frame rate imaging with limited diffraction beams. IEEE Trans Ultrason Ferroelectr Freq Control. 1998;45(1):84-97.
3. Lu J-y, Cheng J, Wang J. High frame rate imaging system for limited diffraction array beam imaging with square-wave aperture weightings high frame rate imaging system for limited diffraction array beam imaging with square-wave aperture weightings. IEEE Trans Ultrason Ferroelectr Freq Control. 2006;53(10):1796-812.
4. Cheng J, Lu J-y. Extended high-frame rate imaging method with limited-diffraction beams. IEEE Trans Ultrason Ferroelectr Freq Control. 2006;53(5):880-9.
5. Kruizinga P, Mastik F, de Jong N, van der Steen AF, van Soest G. Plane-wave ultrasound beamforming using a nonuniform fast Fourier transform. IEEE Trans Ultrason Ferroelectr Freq Control. 2012;59(12):2684-91.
6. Garcia D, Le Tarnec L, Muth S, Montagnon E, Porée J, Cloutier G. Stolt's fk migration for plane wave ultrasound imaging. IEEE Trans Ultrason Ferroelectr Freq Control. 2013;60(9):1853-67.
7. Schwab H-M, Schmitz G. Full-wave ultrasound reconstruction with linear arrays based on a fourier split-step approach. In 2018 IEEE International Ultrasonics Symposium (IUS). New York: IEEE; 2018, pp. 1-4.
8. Stolt RH. Migration by Fourier transform. Geophysics. 1978; 43(1):23-48.
9. Moghimirad E, Hoyos CAV, Mahloojifar A, Asl BM, Jensen JA. Fourier beamformation of multistatic synthetic aperture ultrasound imaging. In 2015 IEEE International Ultrasonics Symposium (IUS). New York: IEEE; 2015, pp. 1-4.
10. Bottenus N. Recovery of the complete data set from focused transmit beams. IEEE Trans Ultrason Ferroelectr Freq Control. 2017;65(1):30-8.
11. Bottenus N. Recovery of the complete data set from ultrasound sequences with arbitrary transmit delays. In Proceedings of Meetings on Acoustics 174ASA, vol 31. Acoustical Society of America; 2017, p. 020001.
12. Ali R, Dahl JJ, Bottenus N. Regularized inversion method for frequency-domain recovery of the full synthetic aperture dataset from focused transmissions. In 2018 IEEE International Ultrasonics Symposium (IUS). New York: IEEE; 2018, pp. 1-9.
13. Ali R, Herickhoff CD, Hyun D, Dahl JJ, Bottenus N. Extending retrospective encoding for robust recovery of the multistatic data set. IEEE Trans Ultrason Ferroelectr Freq Control. 2020; 67(5):943-56.
14. Ali R, Dahl JJ, Bottenus N. Iterative retrospective recovery of full synthetic aperture data from focused transmissions. In 2019 IEEE International Ultrasonics Symposium (IUS). New York: IEEE; 2019, pp. 1005-8.
15. Bae M-H, Jeong M-K. A study of synthetic-aperture imaging with virtual source elements in B-mode ultrasound imaging systems. IEEE Trans Ultrason Ferroelectr Freq Control. 2000; 47(6):1510-9.
16. Moghimirad E, Hoyos CAV, Mahloojifar A, Asl BM, Jensen JA. Synthetic aperture ultrasound Fourier beamformation using virtual sources. IEEE Trans Ultrason Ferroelectr Freq Control. 2016;63(12):2018-30.
17. Loewenthal D, Hu L-z. Two methods for computing the imaging condition for common-shot prestack migration. Geophysics. 1991;56(3):378-81.
18. Schleicher J, Costa JC, Novais A. A comparison of imaging conditions for wave-equation shot-profile migration. Geophysics. 2008;73(6):S219-27.
19. Duan Y, Sava P. Scalar imaging condition for elastic reverse time migration. Geophysics. 2015;80(4):S127-36.
20. Valenciano AA, Biondi B. 2-D deconvolution imaging condition for shot-profile migration. In 2003 SEG Annual Meeting. Society of Exploration Geophysicists, 2003.
21. Biondi B. Short note: equivalence of source-receiver migration and shot-profile migration. Geophysics. 2003;68(4):1340-7.
22. Rao J, Saini A, Yang J, Ratassepp M, Fan Z. Ultrasonic imaging of irregularly shaped notches based on elastic reverse time migration. NDT E Int. 2019;107:102135.
23. Ali R, Jennings J, Dahl JJ. Medical pulse-echo ultrasound imaging based on the cross-correlation of transmitted and backpropagated-receive wavefields. In 2020 IEEE International Ultrasonics Symposium (IUS). New York: IEEE; 2020, pp. 1-4.
24. Goodman JW. Introduction to Fourier optics. Englewood, Colorado: Roberts and Company Publishers; 2005.

25. Jensen JA. Field: a program for simulating ultrasound systems. In 10th Nordicbaltic Conference On Biomedical Imaging, vol 34, supplement 1, part 1. Citeseer; 1996, pp. 351-3.
26. Jensen JA, Svendsen NB. Calculation of pressure fields from arbitrarily shaped, apodized, and excited ultrasound transducers. IEEE Trans Ultrason Ferroelectr Freq Control. 1992;39(2):262-7.
27. Bottenus N. A method for intrapulse spatial compounding. In 2016 IEEE International Ultrasonics Symposium (IUS). New York: IEEE; 2016, pp. 1-4.
28. Stolk CC, de Hoop MV. Modeling of seismic data in the downward continuation approach. SIAM J Appl Math. 2005; 65(4):1388-406.
29. Stolk CC, Maarten V. Seismic inverse scattering in the downward continuation approach. Wave Motion. 2006;43(7):579-98.
30. Bottenus N. Comparison of virtual source synthetic aperture beamforming with an element-based model. J Acoust Soc Am. 2018;143(5):2801-12.
31. Ali R, Dahl JJ. Distributed phase aberration correction techniques based on local sound speed estimates. In 2018 IEEE International Ultrasonics Symposium (IUS). New York: IEEE; 2018, pp. 1-4.
32. Jakovljevic M, Hsieh S, Ali R, Chau Loo Kung G, Hyun D, Dahl JJ. Local speed of sound estimation in tissue using pulse-echo ultrasound: model-based approach. J Acoust Soc Am. 2018;144(1):254-66.
33. Stähli P, Kuriakose M, Frenz M, Jaeger M. Forward model for quantitative pulse-echo speed-of-sound imaging. arXiv preprint arXiv:1902.10639.
34. Jaeger M, Held G, Peeters S, Preisser S, Grünig M, Frenz M. Computed ultrasound tomography in echo mode for imaging speed of sound using pulse-echo sonography: proof of principle. Ultrasound Med Biol. 2015;41(1):235-50.
35. Stoffa PL, Fokkema JT, de Luna Freire R, Kessinger W. Split-step Fourier migration. Geophysics. 1990;55(4):410-21.
36. Gazdag J, Sguazzero P. Migration of seismic data by phase shift plus interpolation. Geophysics. 1984;49(2):124-31.
37. Sava P, Biondi B. Wave-equation migration velocity analysis. I. Theory. Geophys Prospect. 2004;52(6):593-606.